Tetragonal $BiFeO_3$ on yttria-stabilized zirconia

Heng-Jui Liu' , Yu-Hao Du' , Peng Gao, Yen-Chin Huang, Hsiao-Wen Chen, Yi-Chun Chen, Hsiang-Lin Liu, Qing He, Yuichi Ikuhara, and Ying-Hao Chu'

Citation: APL Mater. **3**, 116104 (2015); doi: 10.1063/1.4935310
View online: http://dx.doi.org/10.1063/1.4935310
View Table of Contents: http://aip.scitation.org/toc/apm/3/11
Published by the American Institute of Physics

Tetragonal $BiFeO_3$ on yttria-stabilized zirconia

Heng-Jui Liu,[1,2,a] Yu-Hao Du,[1,a] Peng Gao,[3] Yen-Chin Huang,[4] Hsiao-Wen Chen,[2] Yi-Chun Chen,[4] Hsiang-Lin Liu,[2] Qing He,[5] Yuichi Ikuhara,[3] and Ying-Hao Chu[1,6,b]

[1]*Department of Materials Science Engineering, National Chiao Tung University, Hsinchu 30010, Taiwan*
[2]*Department of Physics, National Taiwan Normal University, Taipei 11677, Taiwan*
[3]*Institute of Engineering Innovation, The University of Tokyo, Tokyo 113-8656, Japan*
[4]*Department of Physics, National Cheng Kung University, Tainan 70101, Taiwan*
[5]*Department of Physics, Durham University, Durham DH1 3LE, United Kingdom*
[6]*Institute of Physics, Academia Sinica, Taipei 11529, Taiwan*

(Received 4 September 2015; accepted 22 October 2015; published online 5 November 2015)

High structural susceptibility of multiferroic $BiFeO_3$ (BFO) makes it a potential replacement of current Pb-based piezoelectrics. In this study, a tetragonal phase is identified based on a combination of x-ray diffraction, scanning transmission electronic microscopy, x-ray absorption spectroscopy, and Raman spectroscopy when BFO is grown on yttria-stabilized zirconia (YSZ) substrates. To distinguish the discrepancy between this tetragonal phase and common cases of monoclinic BFO, piezoelectric force microscopy images and optical property are also performed. It shows a lower electrostatic energy of ferroelectric domains and a large reduction of band gap for BFO grown on YSZ substrate comparing to the well-known one grown on $LaAlO_3$ substrate. Our findings in this work can provide more insights to understand the structural diversity of multiferroic BFO system for further applications. [http://dx.doi.org/10.1063/1.4935310]

In the pursuit of low-power consumption nanoelectronics, advantage of inherently mutual couplings among various coexisting ferroic order parameters in multiferroics make it a potent platform. Among numerous multiferroic systems, $BiFeO_3$ (BFO) is currently the most studied. BFO is an ideal platform for manipulating the lattice, charge, orbital, and spin degrees of freedom via an electric field and therefore serves as a fertile playground for exploring new possibilities for next-generation electronics.[1–8] Recently, through an assistance of strain engineering in thin film process, BFO exhibits a rich variety of phases including rhombohedral, monoclinic, and orthorhombic structures.[9–14] Numerous efforts have also been made to reveal the fundamental understanding of correlation between structure and electric/magnetic order parameters. In the past decade, a great research interest has notably focused on discovering the pseudo-tetragonal phase with large axial ratio (c/a) of ~1.25 that can be only epitaxially stabilized on the substrate with compressive misfit strain greater than 4.5%. This pseudo-tetragonal polymorph can be considered as a new phase and theoretically predicted to have an extremely large polarization ~150 $\mu C/cm^2$.[8,15,16] However, experimental results up to date have never observed a real tetragonal phase of pure BFO, or to be precise, the phase has been confirmed as a monoclinic phase with several possible space groups of *Cc*, *Cm*, *Pm*, or *Pc* symmetry.[10,12,17] Such low-symmetry phases (here labeled as tetragonal-like phase) usually serve as a structural intermediate between rhombohedral and tetragonal phases, which is easily observed in morphotropic phase boundaries (MPBs) of perovskite ferroelectrics.[9–13,18–20] At present, the crystal

[a]H.-J. Liu and Y.-H. Du contributed equally to this work.
[b]Author to whom correspondence should be addressed. Electronic mail: yhc@nctu.edu.tw

structure closest to pure tetragonal has been observed in a very thin film (~7 nm), reported by Pailloux *et al.*[21] Another way is using the modification such as the substitution of Bi ions by Ba ions. This substitution gives a consequence of both the larger ionic radius of Ba^{2+} and the formation of oxygen vacancies and therefore induces a larger effective biaxial compressive stress to successfully gain the pure tetragonal phase.[11] In addition, a recent study[22] has suggested that the symmetry mismatch of substrate and film plays a significant role on BFO crystal and domain structures. Following this concept, we find that the substrates such as $LaAlO_3$ (LAO) and $YaAlO_3$ (YAO) generally used to grow BFO films belong to the distorted perovskite systems, which do not have a cubic symmetry, and thus it possibly leads to the formation of monoclinic phase. In this study, the cubic yttria-stabilized zirconia (YSZ) single crystal substrate has been attempted to grow pure tetragonal BFO (*T*-BFO). Building on the experimental data obtained from a combination of symmetry sensitive techniques such as x-ray diffraction (XRD), scanning transmission electronic microscopy (STEM), x-ray absorption spectroscopy (XAS), Raman spectroscopy, and piezoelectric force microscopy (PFM), we have identified the existence of tetragonal phase in epitaxial films subjected to such stresses.

In order to probe the crystal structure, 50 nm BFO thin film grown on YSZ substrate was characterized by synchrotron-based XRD techniques including a typical $2\theta/\theta$ scan and asymmetric reciprocal space maps (RSMs) at wiggler beamline BL-17B1 of National Synchrotron Radiation Research Center (NSRRC) in Taiwan. The monochromatic beam with energy of 10 keV was focused by a toroidal focusing mirror. The beam size was set to about 0.5×0.6 mm^2 with the scattering vector resolution is around 1×10^{-3} nm^{-1}, which is high enough to resolve any kind of domain structures. As shown in Figure 1(a), merely two diffraction peaks except the YSZ (002) peak are presented in the

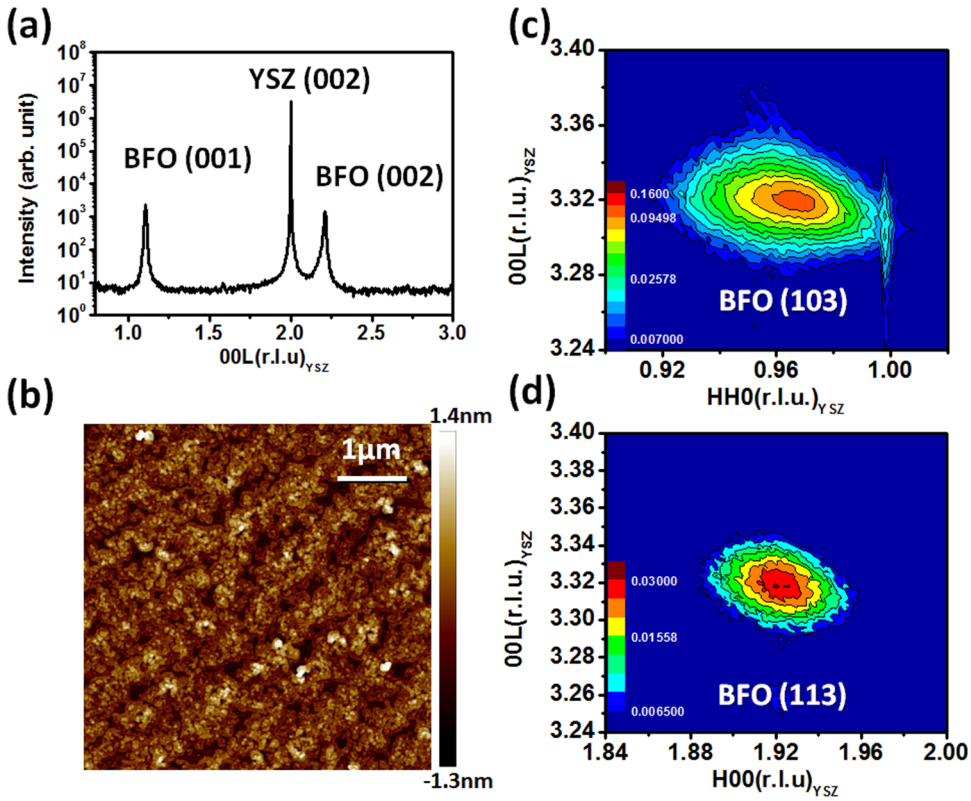

FIG. 1. (a) The high resolution θ-2θ XRD pattern of the BFO thin film grown on the YSZ substrate, which is normalized to the reciprocal unit of YSZ lattice. (b) The morphology of atomic force microscopy (AFM) image shows a smooth surface of BFO thin film. (c) and (d) are the asymmetric x-ray reciprocal space maps taken around the BFO (103) and (113) reflections, respectively, normalized to the reciprocal unit of YSZ lattice as well.

radial scan along surface normal, implying that the BFO film can be grown epitaxially on YSZ substrate without secondary phases. The morphology of a smooth surface of the root-mean-square roughness (R_{rms}) around 3.1 Å is presented in Fig. 1(b), which confirms the high quality growth of the BFO thin film. The out-of-plane lattice constant extracted from the XRD pattern is around 4.65 Å, which is very close to that of BFO tetragonal-like (*T-like*) phase grown on LAO substrates. According to the previous studies, the BFO *T-like* phase has a c/a ratio of ~1.25, which results from a gigantic compressive lattice misfit strain between its bulk form and substrates, where the value is larger than 4.5%.[9–13] However, in our case, the lattice misfit strain between bulk BFO ($a \approx 3.96$ Å) and YSZ ($a = 5.146$ Å) was tensile with a large value of 23% if they followed the cubic-on-cubic growth, which theoretically would not lead to the presence of *T-like* phase. To unveil the observed large c-axis value, the detailed structural information was extracted using asymmetric RSMs recorded in the bases of YSZ reciprocal lattice unit (Figs. 1(c) and 1(d), respectively). From these RSMs, the BFO (103) and (113) reflections both show single peak feature locating at positions of $(0.965\ 0.965\ 3.32)_{YSZ}$ and $(1.93\ 0\ 3.32)_{YSZ}$. The lattice parameters of BFO extracted from RSMs are $a = b = 3.771$ Å and $c = 4.65$ Å and all three axes are orthogonal to each other, clearly indicating that this BFO film might have a tetragonal lattice (here is labeled as *T*-BFO to be distinguished from *T-like* BFO). Additionally, epitaxial orientation relationships between the BFO film and the YSZ substrate are $(001)_{BFO} \,||\, (001)_{YSZ}$ and $[100]_{BFO} \,||\, [110]_{YSZ}$. Such a 45° conjugation between in-plane BFO and YSZ lattice can be ascribed to the smaller lattice mismatch between (110) d-spacing of YSZ and *a*-axis of the *T*-BFO (3.639 Å and 3.771 Å, respectively). More importantly, the RSMs results indeed exhibit different diffraction patterns compared to those of *T-like* phase grown on LAO or YAO substrates. In general, the *T-like* phase with the similar thickness grown on LAO or YAO substrates has been found to possess the monoclinic structure with M_C type symmetry at room temperature. The diffraction characteristic of BFO M_C phase presents three-fold and two-fold splits along its (H0L) and (HHL) RSMs, possessing the lattice structure with *a*-, *b*-, and *c*-axes of 3.81 Å, 3.76 Å, and 4.64 Å, and a tilting angle around 88.5° between the *a*- and *c*-axes.[10–13] Our discovery of *T*-BFO gets very close to the theoretical predictions, though the experimental lattice parameters are still slightly different from the theoretical ones (a = b = 3.665 Å, c = 4.65 Å).[9]

To further realize the interfacial structure and the epitaxial growth mechanism of *T*-BFO thin film on YSZ substrate, atomically resolved Z (atomic number)-contrast imaging from aberration corrected STEM has also been performed along the [100] zone axis of YSZ substrate. As shown in Figure 2(a),

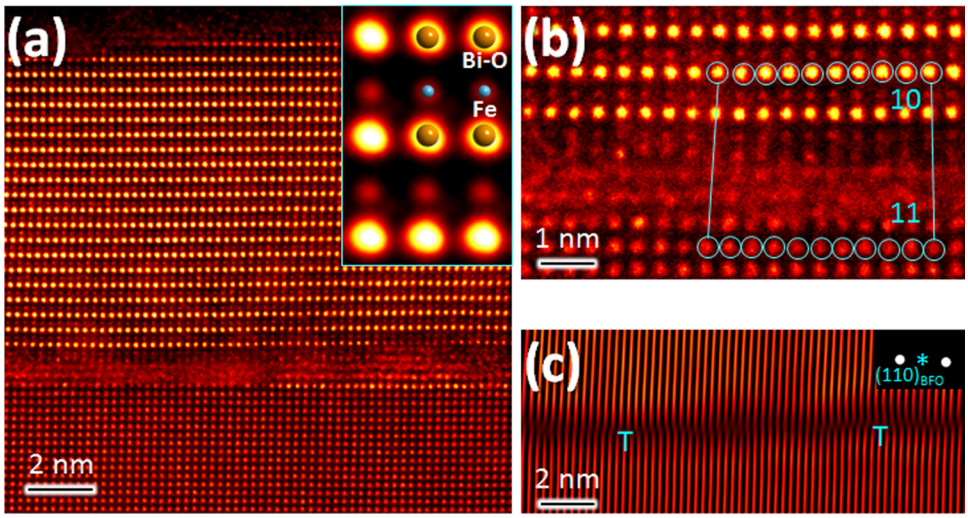

FIG. 2. Atomic structure of $BiFeO_3$ thin film on YSZ substrate. (a) Atomically resolved Z-contrast image along zone axis of $[100]_{YSZ}$ shows the weak bonding between film and substrate at the interface wherein some area has amorphous nature. (b) An enlarged view of interface from left corner of (a). A region with misfit is highlighted. (c) The interface region filtered in Fourier space (inset) by including only the $(100)_{YSZ}$ and $(110)_{BFO}$ lattice plane frequencies. The locations of misfit are roughly highlighted by "T.".

the cross-sectional Z-contrast image implies that *T*-BFO thin film grown on YSZ substrate presents high quality of epitaxial growth. Based on the principle in Z-contrast images, heavier atoms exhibit brighter contrast. We can directly identify Bi and Fe atom columns through the comparison of contrast as the cartoons labeled in the inset of Fig. 2(a). In addition, the in-plane and out-of-plane spacing of *T*-BFO can also be calculated as 2.67 Å and 4.67 Å according to this inset, which can be referred to the d-spacing of (110) and (001) planes of *T*-BFO, respectively. It is also worth to note that the [110] zone axis of *T*-BFO atoms in the HAADF image perfectly aligns with the YSZ [100] axis, which agrees with our XRD observations. Interestingly, such epitaxial relationship seems to be built on a weak bonding between *T*-BFO thin film and YSZ substrate. As shown in Figures 2(a) and 2(b), a nearly amorphous layer with thickness ~2.5 BFO unit cells exists at interface, implying that only a small portion of *T*-BFO can conjugate with YSZ substrate at the initial growth stage. These few crystallized *T*-BFO grains on the surface then act as seeds as well as provide partially strained environment for sequent growth of *T*-BFO epitaxial film. This could be supported by the Fourier space image as shown in Fig. 2(c). Theoretically, if the *T*-BFO thin film is fully relaxed while grown on YSZ substrate, an extra atomic plane should be found about every 28 atomic planes of YSZ, corresponding to 3.5% misfit between *T*-BFO (110) plane and YSZ (200) plane. Nevertheless, as the presence of several edge dislocations unveiled in the Fourier space filtered in Fig. 2(c), we can find an extra atomic plane appears around every 35 atomic planes of YSZ substrate, supporting that *T*-BFO film still sustains the partial constraint from YSZ substrate. Therefore, we may conclude that the overall effects of weak bonding and symmetric in-plane substrate constraint finally lead to stabilize the *T*-BFO phase rather than the *R*-BFO phase.

Such a large tetragonality measured by XRD and STEM is expected to result in five-coordinated Fe sites. In order to confirm this expectation, soft XAS and the corresponding X-ray linear dichroism (XLD) measurements have been employed to investigate the detailed electronic structure and crystal field splitting of this phase. The XAS-LD spectra were collected at the Dragon beamline of the NSRRC in Taiwan. With the photon energy scanned across the Fe $L_{2,3}$ absorption edges,[23,24] linearly polarized x-rays were shined to the *T*-BFO sample with the electric field (E) vector parallel or perpendicular to the *c* axis of the crystal ($E//a$ or $E//c$). In the Fe $L_{2,3}$ spectra (Fig. 3(a)), the L_3 edge (~708.6 eV) and the L_2 edge (~722.1 eV) are caused by excitations from the Fe $2p_{3/2}$ and Fe $2p_{1/2}$ states into empty Fe 3*d* states, respectively. Both edges exhibit doublet peaks, of which the main peak and prepeak correspond to the higher e_g energy level (x^2-y^2, $3z^2$-r^2) and lower lying t_{2g} energy level (*xy*, *yz*, *xz*) that are induced by a octahedral crystal field.[25] It is important to note that there is a considerable polarization dependence in the XAS line shape: both peak intensity changes and peak energy shifts have been observed. The relative intensity changes at various peaks mainly arise from "magnetic linear dichroism,"[26–29] while the observed peak energy shifts of several tenths of an eV are mainly attributed "crystal field dichroism."[30–32] The energy shift of the L_3 main peak is about ~−0.24 eV, while for the L_3 prepeak, it is ~+0.13 eV when the x-ray polarization goes from $E//a$ to $E//c$. Such result indicates that the $3z^2$-r^2 orbital is likely to be lower in energy comparing to the x^2-y^2 orbital, and the energy of the *xz*-*zy* orbital is higher than the *xy* orbital. The opposite energy shift observed in main peak and prepeak has been attributed to off-centering of Bi and Fe ions in the O octahedron, leading to a square pyramid (5-fold) coordination.[21,25,33] More obvious evidence can be revealed in XLD spectrum, which is obtained from the intensity difference ($I_{E//a} - I_{E//c}$) between the normalized XAS spectra of $E//a$ and $E//c$. The variation in XLD spectrum is similar to the previous studies on triclinic phases with large c/a ratio, confirming again the large crystal elongation along c-axis for this T-BFO film.[33] In addition, the symmetry of this *T*-BFO grown on YSZ was probed by Raman spectroscopy. Fig. 3(b) shows the comparison of Raman spectra of BFO grown on LAO and YSZ substrates. Both substrate phonons have been deducted from the original spectra. Phonon peaks of BFO on LAO are located at 145, 224, 243, 273, 361, 589, and 689 cm^{-1}, which belong to the monoclinic *Cc* symmetry, as reported in the previous study of *T*-like BFO films.[34] In contrast to the large number of Raman active modes of the *Cc* structure (14A′ + 13A″), only eight Raman peaks ($3A_1 + B_1 + 4E$) are expected in the case of tetragonal *P4mm* symmetry. In our backward scattering measurement setup, the incident and scattering light are along the (001) direction of the sample, which means no z components of light polarizations. The polarization selection rules of *P4mm* in this configuration eliminate the scattering possibility of E modes and further reduce the observable peaks to 4

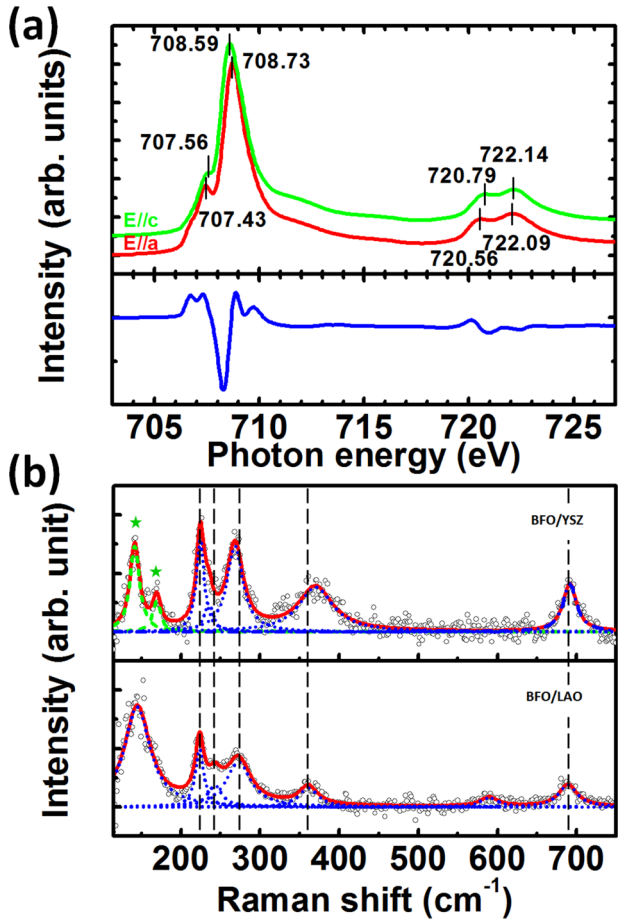

FIG. 3. (a) Fe $L_{3,2}$-edge X-ray absorption spectra (XAS) of T-BFO thin film are measured at different polarizations (E//a and E//c) and the corresponding X-ray linear dichroism (XLD) is extracted from normalized intensity difference ($I_{E//a} - I_{E//c}$). (b) Raman spectra of BFO/YSZ and BFO/LAO.

modes ($3A_1 + B_1$). In Fig. 3(b), at least 7 peaks are needed to fit the Raman spectrum of the BFO film grown on YSZ, which shows the lower symmetry than *P4mm* in BFO/YSZ microstructure. However, discrepancies between Raman spectra of BFO/YSZ and BFO/LAO still indicate the difference of their crystal structure. In these two films, the high-frequency phonon modes at 690 cm^{-1} are nearly the same while most low-frequency peaks have significant shifts. Moreover, in contrast to the lowest observable phonon of BFO/LAO films at 145 cm^{-1}, phonons of BFO/YSZ below 200 cm^{-1} split into two peaks, 142 and 169 cm^{-1} (starred in green). The low-frequency modes are related to vibrations between Bi cations and FeO_6 octahedra, so their changes imply different tilting angles of the oxygen octahedra or Bi-O bondings. As a consequence, physical properties are expected to be different in BFO/LAO and BFO/YSZ.

From the analysis of Raman spectra, this T-BFO seems not to possess the *P4mm* symmetry. It suggests a deviation of ferroelectric polarization from c-axis. In order to probe the direction of ferroelectric polarization, PFM has been employed to directly measure BFO films grown on YSZ and LAO without bottom electrode. The in-plane PFM images (Figs. 4(a) and 4(b)) show that BFO films grown on YSZ and LAO have similar domain structures. Both domains form periodic strips with in-plane polarization components projecting along ⟨100⟩ directions of BFO crystal. The domain width of BFO/YSZ is about 25 nm, while the domain width of BFO/LAO is about 15 nm. The larger domain width indicates better electrostatic compensation (or lower electrostatic energy) of domain in BFO/YZS, suggesting a smaller in-plane component of ferroelectric component either results from a

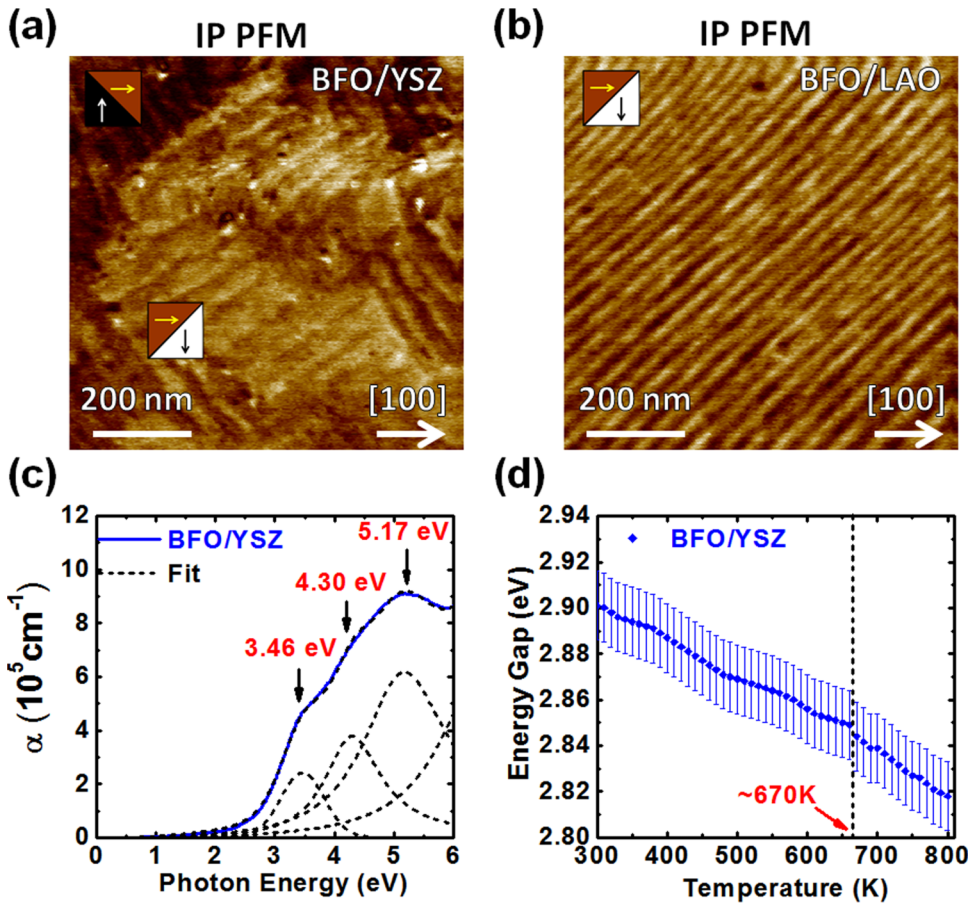

FIG. 4. (a) and (b) are the in-plane piezoresponse force microscope images of BFO/YSZ and BFO/LAO, respectively. The insets show the directions of in-plane polarization components. (c) Room-temperature optical absorption coefficient of a *T*-BFO film. Four fitted Lorentzian oscillators in black dashed lines are also shown. (d) Temperature dependent band gap of a *T*-BFO film. The vertical dashed lines denote the anomalies.

smaller magnitude of total spontaneous ferroelectric polarization or a smaller deviation of ferroelectric axis from *c*-axis. We have found out that several possible symmetries, such as *P4bm*, $P4_2/nmc$, and *I4*/*mcm*, in tetragonal perovskites may offer the solutions for the observed in-plane polarization.[35] For example, lead-free ferroelectric $Na_{0.5}Bi_{0.5}TiO_3$ has tilted oxygen octahedrons in a tetragonal lattice with *P4bm* symmetry at 698 K.[36] $SrSnO_3$ also shows the *I4*/*mcm* symmetry at above 1073 K.[37] However, to fully understand the detailed relationship between structure and polarization property of *T*-BFO in this work still need further theoretical support.

Spectroscopic ellipsometric measurements were performed at various angles of incidence between 60° and 75° using a Woollam M-2000U ellipsometer over the spectral range 0.73-6.42 eV to study the optical property of this *T*-BFO. The reproducibility of the spectra was confirmed at different regions on the film surface by using a combination of specially designed focusing optics and spectroscopic ellipsometry for spot ($100 \times 100\ \mu m^2$) measurements. The complex dielectric functions of a *T*-BFO were extracted by fitting the ellipsometric spectra using the stacked layer model consisting of YSZ substrate/BFO film/surface roughness/air ambient structure. The thin films were placed in a LINKAM heating vacuum stage system, which enabled measurements in the temperature range of 300-800 K. To deal with the dispersion and absorption in YSZ substrate, its temperature-dependent ellipsometric spectra were also measured. Figure 4(c) shows the room-temperature optical absorption spectrum of a *T*-BFO determined from spectroscopic ellipsometric analysis. The absorption starts to gradually increase above 1.0 eV, manifests a sharp rise from 3.0 eV, reaches a maximum value about 5.17 eV, and then levels off. After carefully fitting the absorption data using a classical Lorentzian

model, we have assigned the 3.46, 4.30, and 5.17 eV peaks to minority channel dipole-allowed charge transfer electronic excitations.[38–40] The direct band gap of a *T*-BFO thin film was extracted by a linear extrapolation of an $(\alpha \cdot E)^2$ versus E plot to zero.[41] The band gap in a *T*-BFO thin film is approximately 2.89 ± 0.01 eV, which is significantly smaller than that of *T-like* BFO on LAO (~3.12 eV)[42] and larger than that of *R*-BFO on STO (2.77–2.82 eV).[42,43] Noteworthily, it has been known that the band gap of BFO is almost independent to its strain when it is still keeps the same phase.[43] Therefore, it implies that the observed difference in energy gap is phase-dependent, suggesting that the *T*-BFO found in this study should be different, the common cases of *T-like* BFO. Moreover, with an increase in the temperature, an anomaly in the band gap was observed at approximately 670 K (Fig. 4(d)). This anomaly could be associated with the antiferromagnetic phase transition temperature of a *T*-BFO thin film.

To sum up, by taking a large lattice mismatch and cubic symmetry YSZ substrate, *T*-BFO is successfully fabricated and evidenced by XRD, STEM, and XAS. However, a symmetry sensitive measurement such as Raman spectra suggests this phase possess a lower symmetry rather than a typically symmetry, *P4mm*, in traditional tetragonal ferroelectrics. Such a lower symmetry makes this *T*-BFO have the similar ferroelectric domain structure to the case of monoclinic BFO. Interestingly, although the resembled domain structure for both tetragonal and monoclinic phases is observed, optical property from spectroscopic ellipsometric measurements still demonstrates an obvious difference of band gap between them: a large reduction of bandgap is characterized for BFO grown on YSZ compared to the one on LAO. This study adds a new structural variation and gives a further insight into important multiferroic field.

The authors acknowledge the support of the Ministry of Science and Technology under Grant No. MOST 103-2119-M-009-003-MY3 and MOST 102-2112-M-006-008-MY3.

[1] R. Ramesh and N. A. Spaldin, Nat. Mater. **6**, 21 (2007).
[2] F. Zavaliche, S. Y. Yang, T. Zhao, Y. H. Chu, M. P. Cruz, C. B. Eom, and R. Ramesh, Phase Transitions **79**, 991 (2006).
[3] G. Catalan and J. F. Scott, Adv. Mater. **21**, 2463 (2009).
[4] D. Sando, A. Barthélémy, and M. Bibes, J. Phys.: Condens. Matter **26**, 473201 (2014).
[5] S.-Y. Yang, F. Zavaliche, L. Mohaddes-Ardabili, V. Vaithyanathan, D. G. Schlom, Y.-J. Lee, Y.-H. Chu, M. P. Cruz, Q. Zhan, T. Zhao, and R. Ramesh, Appl. Phys. Lett. **87**, 102903 (2005).
[6] B. Kundys, M. Viret, D. Colson, and D. O. Kundys, Nat. Mater. **9**, 803 (2010).
[7] J.-C. Yang, C.-H. Yeh, Y.-T. Chen, S.-C. Liao, R. Huang, H.-J. Liu, C.-C. Hung, S.-H. Chen, S.-L. Wu, C.-H. Lai, Y.-P. Chiu, P.-W. Chiu, and Y.-H. Chu, Nanoscale **6**, 10524 (2014).
[8] J. Wang, J. B. Neaton, H. Zheng, V. Nagarajan, S. B. Ogale, B. Liu, D. Viehland, V. Vaithyanathan, D. G. Schlom, U. V. Waghmare, N. A. Spaldin, K. M. Rabe, M. Wuttig, and R. Ramesh, Science **299**, 1719 (2003).
[9] R. J. Zeches, M. D. Rossell, J. X. Zhang, A. J. Hatt, Q. He, C.-H. Yang, A. Kumar, C. H. Wang, A. Melville, C. Adamo, G. Sheng, Y.-H. Chu, J. F. Ihlefeld, R. Erni, C. Ederer, V. Gopalan, L. Q. Chen, D. G. Schlom, N. A. Spaldin, L. W. Martin, and R. Ramesh, Science **326**, 977 (2009).
[10] A. R. Damodaran, C.-W. Liang, Q. He, C.-Y. Peng, L. Chang, Y.-H. Chu, and L. W. Martin, Adv. Mater. **23**, 3170 (2011).
[11] H. M. Christen, J. H. Nam, H. S. Kim, A. J. Hatt, and N. A. Spaldin, Phys. Rev. B **83**, 144107 (2011).
[12] H.-J. Liu, C.-W. Liang, W.-I. Liang, H.-J. Chen, J.-C. Yang, C.-Y. Peng, G.-F. Wang, F.-N. Chu, Y.-C. Chen, H.-Y. Lee, L. Chang, S.-J. Lin, and Y.-H. Chu, Phys. Rev. B **85**, 014104 (2012).
[13] H.-J. Liu, H.-J. Chen, W.-I. Liang, C.-W. Liang, H.-Y. Lee, S.-J. Lin, and Y.-H. Chu, J. Appl. Phys. **112**, 052002 (2012).
[14] J.-C. Yang, Q. He, S. J. Suresha, C.-Y. Kuo, C.-Y. Peng, R. C. Haislmaier, M. A. Motyka, G. Sheng, C. Adamo, H.-J. Lin, Z. Hu, L. Chang, L. H. Tjeng, E. Arenholz, N. J. Podraza, M. Bernhagen, R. Uecker, D. G. Schlom, V. Gopalan, L.-Q. Chen, C.-T. Chen, R. Ramesh, and Y.-H. Chu, Phys. Rev. Lett. **109**, 247606 (2012).
[15] R. Dan, K.-Y. Yun, and M. Okuyama, J. Phys.: Condens. Matter **18**, L97 (2006).
[16] H. Béa, B. Dupé, S. Fusil, R. Mattana, E. Jacquet, B. Warot-Fonrose, F. Wilhelm, A. Rogalev, S. Petit, V. Cros, A. Anane, F. Petroff, K. Bouzehouane, G. Geneste, B. Dkhil, S. Lisenkov, I. Ponomareva, L. Bellaiche, M. Bibes, and A. Barthélémy, Phys. Rev. Lett. **102**, 217603 (2009).
[17] O. Diéguez, O. E. González-Vázquez, J. C. Wojdeł, and J. Íñiguez, Phys. Rev. B **83**, 094105 (2011).
[18] H. Fu and R. E. Cohen, Nature **403**, 281 (2000).
[19] M. Ahart, M. Somayazulu, R. E. Cohen, P. Ganesh, P. Dera, H.-K. Mao, R. J. Hemley, Y. Ren, P. Liermann, and Z. Wu, Nature **451**, 545 (2008).
[20] T. Asada and Y. Koyama, Phys. Rev. B **75**, 214111 (2007).
[21] F. Pailloux, M. Couillard, S. Fusil, F. Bruno, W. Saidi, V. Garcia, C. Carrétéro, E. Jacquet, M. Bibes, A. Barthélémy, G. A. Botton, and J. Pacaud, Phys. Rev. B **89**, 104106 (2014).
[22] Z.-H. Chen, A. R. Damodaran, R. Xu, S. Lee, and L. W. Martin, Appl. Phys. Lett. **104**, 182908 (2014).
[23] Q. He, Y.-H. Chu, J. T. Heron, S.-Y. Yang, W.-I. Liang, C.-Y. Kuo, H.-J. Lin, P. Yu, C.-W. Liang, R. J. Zeches, W.-C. Kuo, J.-Y. Juang, C.-T. Chen, E. Arenholz, A. Scholl, and R. Ramesh, Nat. Commun. **2**, 225 (2011).
[24] A. Tanaka and T. Jo, J. Phys. Soc. Jpn. **63**, 2788 (1994).
[25] J. X. Zhang, Q. He, M. Trassin, W. Luo, D. Yi, M. D. Rossell, P. Yu, L. You, C. H. Wang, C. Y. Kuo, J. T. Heron, Z. Hu, R. J. Zeches, H. J. Lin, A. Tanaka, C. T. Chen, L. H. Tjeng, Y. H. Chu, and R. Ramesh, Phys. Rev. Lett. **107**, 147602 (2011).

[26] P. Kuiper, B. G. Searle, P. Rudolf, L.-H. Tjeng, and C.-T. Chen, Phys. Rev. Lett. **70**, 1549 (1993).
[27] F. Nolting, A. Scholl, J. Stohr, J. W. Seo, J. Fompeyrine, H. Siegwart, J. P. Locquet, S. Anders, J. Luning, E. E. Fullerton, M. F. Toney, M. R. Scheinfein, and H. A. Padmore, Nature **405**, 767 (2000).
[28] D. Alders, L.-H. Tjeng, F. C. Voogt, T. Hibma, G. A. Sawatzky, C.-T. Chen, J. Vogel, M. Sacchi, and S. Iacobucci, Phys. Rev. B **57**, 11623 (1998).
[29] E. Arenholz, G. van der Laan, R. V. Chopdekar, and Y. Suzuki, Phys. Rev. B **74**, 094407 (2006).
[30] S. I. Csiszar, M. W. Haverkort, Z. Hu, A. Tanaka, H. H. Hsieh, H. J. Lin, C. T. Chen, T. Hibma, and L. H. Tjeng, Phys. Rev. Lett. **95**, 187205 (2005).
[31] N. Hollmann, Z. Hu, T. Willers, L. Bohatý, P. Becker, A. Tanaka, H. H. Hsieh, H. J. Lin, C. T. Chen, and L. H. Tjeng, Phys. Rev. B **82**, 184429 (2010).
[32] M. W. Haverkort, S. I. Csiszar, Z. Hu, S. Altieri, A. Tanaka, H. H. Hsieh, H. J. Lin, C. T. Chen, T. Hibma, and L. H. Tjeng, Phys. Rev. B **69**, 020408 (2004).
[33] K.-T. Ko, M. H. Jung, Q. He, J. H. Lee, C. S. Woo, K. Chu, J. Seidel, B.-G. Jeon, Y. S. Oh, K. H. Kim, W.-I. Liang, H.-J. Chen, Y.-H. Chu, Y. H. Jeong, R. Ramesh, J.-H. Park, and C.-H. Yang, Nat. Commun. **2**, 567 (2011).
[34] M. N. Iliev, M. V. Abrashev, D. Mazumdar, V. Shelke, and A. Gupta, Phys. Rev. B **82**, 014107 (2010).
[35] M. W. Lufaso and P. M. Woodward, Acta Crystallogr., Sect. B: Struct. Sci. **57**, 725 (2001).
[36] G. O. Jones and P. A. Thomas, Acta Crystallogr., Sect. B: Struct. Sci. **56**, 426 (2000).
[37] E. H. Mountstevens, S. A. T. Redfern, and J. P. Attfield, Phys. Rev. B **71**, 220102 (2005).
[38] J. B. Neaton, C. Ederer, U. V. Waghmare, N. A. Spaldin, and K. M. Rabe, Phys. Rev. B **71**, 014113 (2005).
[39] S. R. Basu, L. W. Martin, Y.-H. Chu, M. Gajek, R. Ramesh, R. C. Rai, X. Xu, and J. L. Musfeldt, Appl. Phys. Lett. **92**, 091905 (2008).
[40] X.-S. Xu, T. V. Brinzari, S. Lee, Y.-H. Chu, L. W. Martin, A. Kumar, S. Mcgill, R. C. Rai, R. Ramesh, V. Gopalan, S. W. Cheong, and J. L. Musfeldt, Phys. Rev. B **79**, 134425 (2009).
[41] J. I. Pankove, *Optical Processes in Semiconductors* (Dover, New York, 1971).
[42] H. L. Liu, M. K. Lin, Y. R. Cai, C. K. Tung, and Y. H. Chu, Appl. Phys. Lett. **103**, 181907 (2013).
[43] J. F. Ihlefeld, N. J. Podraza, Z. K. Liu, R. C. Rai, X. Xu, T. Heeg, Y. B. Chen, J. Li, R. W. Collins, J. L. Musfeldt, X. Q. Pan, J. Schubert, R. Ramesh, and D. G. Schlom, Appl. Phys. Lett. **92**, 142908 (2008).